Influence of thin film for LIPSS formation on soda-lime glass using SHG femtosecond laser beam

K. Deva Arun Kumar, Barthélemy Aspe, Martin Depardieu, Anne-Lise Thomann, Nadjib Semmar

RESEARCH ARTICLE | OCTOBER 02 2024

Influence of thin film for LIPSS formation on soda-lime glass using SHG femtosecond laser beam

K. Deva Arun Kumar ; Barthélemy Aspe ; Martin Depardieu; Anne-Lise Thomann ; Nadjib Semmar

AIP Advances 14, 105105 (2024)
https://doi.org/10.1063/5.0230358

Influence of thin film for LIPSS formation on soda-lime glass using SHG femtosecond laser beam

Cite as: AIP Advances 14, 105105 (2024); doi: 10.1063/5.0230358
Submitted: 23 July 2024 • Accepted: 16 September 2024 •
Published Online: 2 October 2024

K. Deva Arun Kumar,[1] Barthélemy Aspe,[1] Martin Depardieu,[2] Anne-Lise Thomann,[1] and Nadjib Semmar[1,a)]

AFFILIATIONS

[1] Groupe de Recherches sur l'Énergétique des Milieux Ionisés, GREMI, Université d'Orléans, CNRS, 14 Rue d'Issoudun, 45067 Orleans, France
[2] Décor World Services (DWS), 1 Av. du Champ de Mars, 45100 Orléans, France

[a)] **Author to whom correspondence should be addressed:** nadjib.semmar@univ-orleans.fr

ABSTRACT

This investigation focuses on the influence of thin films on laser-induced periodic surface structures (TF-LIPSSs) formed on soda-lime glass using femtosecond laser pulses with a wavelength of 515 nm. In this study, we introduce a new framework involving a combined metal thin film of chromium and silver (Cr:30 nm + Ag:100 nm) deposited onto soda-lime glass by DC magnetron sputtering. Due to their better coupling by heat accumulation, metal thin film enables a more efficient transfer of energy to the dielectric glass substrate, leading to the formation of periodic structures. The thin-metal-film-deposited glass substrate is irradiated with the second-harmonic generator of a Satsuma laser source to create the LIPSS at high repetition rates ranging from 10 to 250 kHz. We observe simultaneously low-spatial-frequency LIPSS (LSFL) with a spatial period (Λ) of 400 nm and high-spatial-frequency LIPSS (HSFL) with a spatial period of about 110 nm on thin film and glass substrate, respectively. Interestingly, at 10 μJ and 100 kHz, the HSFL observed on the glass substrate are significantly smaller than half of the irradiation wavelength. In the center region, the $HSFL_{\perp}$ are perpendicular to the laser beam polarization. In the transitioned region between the impact center and the melted area, the $HSFL_{II}$ are parallel to the polarization. Furthermore, when the energy was increased from 10 to 15 μJ, the irradiated zone geometry changed from a regular circular shape to an elliptical one due to an uneven energy distribution over the ablated area, resulting in the formation of irregular surface structures. Finally, a comparative analysis of surface modifications on a metal thin-film-coated glass substrate using different repetition rates and energy levels revealed dissimilar morphological structures.

I. INTRODUCTION

Laser technology for thin film texturing on transparent glass surfaces is crucial within the realm of large-area optical communications. Laser designing offers numerous advantages over conventional lithography-based techniques, as it facilitates the creation of clean, adaptable, and extensive patterns across various materials.[1] In thin-film texturing, short-pulse lasers ranging from nanoseconds to femtoseconds in duration have conventionally been preferred.[2] However, the rise of robust, high-power-density, ultra-short laser sources presents alternatives to the more established nanosecond laser sources. Because of their exceptionally short-pulse durations, femtosecond (fs) lasers utilize multi-photon absorption and electron plasma for material removal.[3,4] Moreover, femtosecond lasers provide better accuracy with less thermal damage, making them flexible tools for producing periodic structures within transparent (wide bandgap) substrates and on the surfaces of various other substrates.[5,6]

The potential to achieve micro-/nanostructuring on various substrates using laser irradiation has directed global attention toward the generation of laser-induced periodic surface structures (LIPSS). They have a significant impact on various applications thanks to their ability to improve surface properties, especially in hydrophobicity and cellular defect variation.[7] In the last two

decades, the LIPSS formation emerged as a promising method in a variety of materials, including metals, semiconductors, and dielectrics. The different parameters of a fs-laser, including repetition rate, fluence, polarization, and spatial distribution, prove to be effective in producing high-quality LIPSS. Two distinct types of LIPSS are typically observed when fs-laser pulses irradiate the surfaces of solid materials: (i) high-spatial-frequency LIPSS (HSFL) and (ii) low-spatial-frequency LIPSS (LSFL). These structures are aligned either perpendicular or parallel to the electric field (**E**) of the laser beam.[8]

It is well known that the materials bandgap significantly influences the nature of the interaction and the LIPSS formation, particularly under sub-ablation conditions or with low-wavelength laser beams. For example, HSFL are primarily observed when the material surface is irradiated with photons whose energy is below the materials bandgap.[9,10] For HSFL, it has been suggested that mechanisms such as specific plasmon modes and self-organization are involved in the context of second-harmonic generation (SHG) laser sources.[11] Recent studies have investigated the LIPSS formation in air environments upon femtosecond laser pulse irradiation of dielectric materials, with a particular focus on fused silica.[12,13] Most dielectric materials have shown HSFL with spatial periods ranging from ~75 to 350 nm.[8] The investigation of the LIPSS formation on dielectric glass substrates is more challenging as it is influenced by the chemical composition of the glasses. Graf *et al.*[14] conducted a systematic investigation of the LIPSS formation on dielectric materials, including fused silica, borosilicate, and soda-lime silicate glass, using femtosecond-IR laser radiation. Both LSFL and HSFL were observed on fused silica and borosilicate glass substrates, while on soda-lime silicate glass, HSFL were barely visible due to the extensive melt formation. Up until now, there have been no reports on the LIPSS formation on soda-lime glass due to its strongly nonlinear absorption behavior.

The choice of glass substrate is important across a wide range of high-tech applications, including solar cells, microfluidics, optics, and biomaterial devices.[15] A well-known glass material is soda-lime silicate, recognized for its cost-effectiveness, good stability, and excellent mechanical properties.[16] Recently, we reported the LIPSS formation on a soda-lime glass substrate using a femtosecond-IR (λ = 1030 nm) laser beam in conjunction with a thin metallic film.[8] However, applications based on visible wavelengths could be more interesting compared to those using IR, for safety and beam shaping in industry, as well as open new surface features with smaller LIPSS sizes.

Despite the limited literatures on dielectric surface modification using a 515 nm laser wavelength compared to IR (1030 nm) wavelengths, this study provides a detailed examination of the effects. Kuzmin and Klekovkin[17] reported a systematic investigation of the structuring and ablation of a titanium film coated on a silicon (Si-100) substrate by fs-laser pulses at 515 nm in both single-pulse and multi-pulse modes. Nevertheless, they observed only periodic surface structures (PSS) on the surface of the Ti thin film, attributed to inadequate energy distribution. This occurs because the energy of each pulse does not exceed the thresholds for spallation ablation and surface wave excitation. A further increase in the energy/number of pulses leads to a notable surpassing of the threshold for generating surface structures in the crater center, resulting in the destruction of ordered structures and the formation of molten regions. Alternatively, Danilov *et al.*[18] examined the femtosecond (Yb:fiber) laser ablation of silver (Ag 50 nm) thin film deposited on a glass substrate at a wavelength of 515 nm. They noticed the development of a round crater with thin walls, along the edges of which sections of film detach from the glass substrate at a pulse energy of around 1.3 μJ. As the pulse energy increases, the size of the crater expands noticeably. It is worth mentioning that there are no signs of melting around the crater's edges, nor is there a melted ridge, suggesting a "cold" mechanism for the separation of silver from the substrate.[19] In both scenarios, there was no detection of LIPSS on either Si or glass substrate, despite the use of a metal thin-film layer.

In this work, we investigate the LIPSS formation on a dielectric soda-lime glass substrate using a Satsuma laser source at 515 nm. For this study, we deposited a combined metal thin film (Ag + Cr) layer on the glass substrate to absorb the femtosecond laser light, facilitating the interaction between the laser beam and the substrate. To the best of our knowledge, there are no reports on the LIPSS formation on a dielectric substrate using a 515 nm laser source. Therefore, we explored and developed new methods in the experimental process to create LIPSS on the glass substrate. In general, metal thin films possess strong absorption properties, allowing them to interact with laser light and facilitate the formation of periodic structures on the glass substrate. We examine the effect of repetition rate and pulse energy on the formation of both LSFL and HSFL, as well as their period sizes, on the glass surface and thin-film layer. The morphology of the LIPSS was studied in detail by varying the pulse energy (i.e., beam fluence). This study highlights the importance of metal thin films for dielectric surface modification and offers insights into the complex processes that lead to LIPSS formation.

II. MATERIALS AND METHODS

In this study, we examined the generation of LIPSS on a glass substrate using fs-laser pulses with second-harmonic generation (λ = 515 nm) under atmospheric conditions. The choice of a dielectric soda-lime glass substrate is due to its superior optical properties compared to absorbing materials such as metals or semiconductors. The LIPSS formation on a glass substrate was achieved using a novel approach involving a combined metal thin-film layer. The strong absorption capability of the metal thin film allows for the efficient transfer of photon energy to the glass substrate, enhancing the interaction between the laser beam and the substrate. Consequently, the LIPSS formation occurs due to the generation of surface plasmon polaritons (SPPs) at the interface between the air and the substrate, as reported by Sládek *et al.*[20]

A 30 nm thick layer of chromium (Cr) and a 100 nm thick layer of silver (Ag) were deposited onto a soda-lime glass substrate using DC sputtering from Cr and Ag targets, respectively, with a substrate thickness of ≥3 mm. Both metal thin-film depositions were conducted at a pressure of 0.5 Pa, using 20 SCCM of Ar as the sputtering gas, with the power set to 200 W for Cr and 50 W for Ag. The deposition time for each layer was 36 s for Cr and 90 s for Ag. The distance between the substrate and the target was ~10 cm. The chromium layer was deposited before the silver layer to enhance the adhesion of the silver to the substrate.

For this study, we employed a Satsuma femtosecond laser (Yb:YAG) operating at a wavelength of 515 nm (SHG), with

the repetition rates ranging from 10 to 250 kHz, and a pulse duration of 300 fs. The pulse energy was varied between 10 and 20 μJ, with a stability period of ~10 min. Linearly polarized laser pulses with a Gaussian beam spatial profile (M^2 ~ 1.08) and a beam diameter of ~2.5 mm at the lens were used to irradiate the sample surface. During irradiation, the beam diameter reached about 35 μm, with a calculated focal depth of 1.6 mm. Calibration procedures were completed prior to the experiments. We performed the laser texturing with a process time of 1 s for the entire range of repetition rates (10–250 kHz from an external acoustic-optic modulator), resulting in N = 10 000 to 250 000 pulses. In our previous work, we comprehensively discussed the experimental process, accompanied by a schematic diagram.[8] In this study, fs-laser processing was conducted in static mode using a wavelength of 515 nm, thanks to the SHG module. Various combinations of fs-laser repetition rate (f), laser fluence (F), and energy (E) were selected as parameters to study the generation of LIPSS on the glass substrate. The optimal experimental procedures were repeated several times to confirm their consistency and reproducibility for future studies.

Three main characterizations were conducted in this study: (i) scanning electron microscopy with a field emission gun (SEM-FEG), using a Zeiss Supra 40 equipped with a secondary electron detector and an accelerating voltage ranging from 1 to 5 kV. Prior to SEM imaging, a 4 nm thick layer of platinum was sputtered onto the laser irradiated glass substrate using a Leica sputter coater to prevent charging effects. (ii) Energy dispersive x-ray spectroscopy (EDX) was conducted at an accelerating voltage of 10 kV to confirm the elemental composition of both the thin film and the glass substrate. (iii) Atomic force microscopy (AFM) using a Bruker Dimension Icon was employed to analyze the amplitude and periodicity of the LIPSS.

III. RESULTS AND DISCUSSION

A. LIPSS on thin film and glass substrate (LSFL and HSFL)

To increase the fs-laser beam absorption onto the glass substrate, we used high repetition rates ranging from 10 to 250 kHz, coupled with energies exceeding 10 μJ as optimized in our previous study.[8] LIPSS were observed on the surfaces of both thin film and soda-lime glass when subjected to multiple pulses with a pulse duration (τ_p) of 300 fs, a wavelength (λ) of 515 nm, and a pulse fluence (F) of 2 J/cm^2. Figure 1 illustrates the LIPSS formation observed through scanning electron microscopy (SEM) at an energy (E) of 10 μJ and a frequency (repetition rate, f) of 100 kHz. Within the localized impact area of ~35 μm, SEM images (Fig. 1) at higher resolution reveal the presence of three nearly circular concentric zones, with two originating from the glass substrate and one from the thin-film layer as we confirmed by chemical analysis. Notably, laser-induced surface features of LSFL$_\perp$ were observed at the periphery of the laser spot, precisely on the thin-film (Ag) layer, exhibiting an orientation perpendicular to the polarization (**E**). This alignment correlates with lower energy density—a fact that can be determined by the

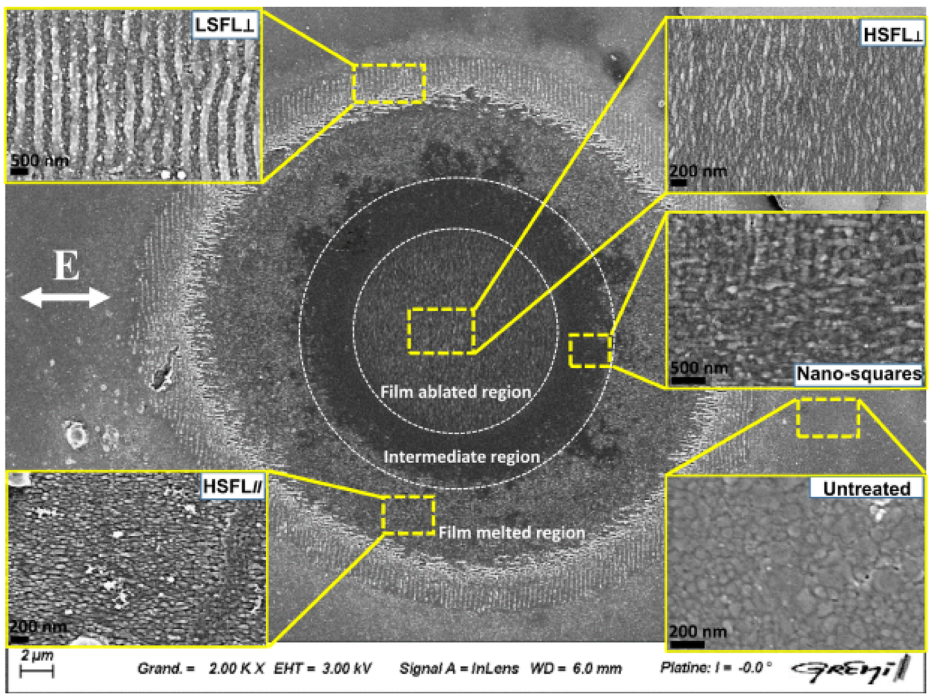

FIG. 1. SEM image of the LIPSS formation at E = 10 μJ for 100 kHz. The insets show the non-irradiated (untreated) surface of thin films (Cr + Ag) and two different LIPSS patterns (HSFL$_{//}$ and *HSFL*$_\perp$) observed from the soda-lime glass and *LSFL*$_\perp$ formed on the thin-film surface.

Gaussian distribution over the laser beam. Farid *et al.*[21] observed surface structures on the periphery of the laser spot on an ITO thin-film-coated glass substrate when exposed to an IR laser beam. This phenomenon is due to the non-uniform temperature distribution caused by heating a confined region with the Gaussian-shaped laser spot, resulting in the build-up of high compressive stresses. These compressive stresses act on the interfaces at grain boundaries and between the irradiated and non-irradiated areas. Dostovalov *et al.*[22] observed LSFL on the surface of a 28 nm Cr thin film under an IR laser beam, with the patterns oriented parallel to the polarization. It is important to note that the LSFL produced in this study extend above the initial surface of the film, unlike those formed under strong ablation conditions. The formation of LSFL is attributed to the initiation of the laser beam on the metallic film surface and the efficient periodic oxidation of the metal in regions of maximum light absorption.[22] The specific "thermochemical" conditions leading to the oxidation during irradiation of metal film surfaces were also investigated by Oktem *et al.*[23] on Ti thin film.

Interestingly, the glass substrate displays two different orientations of HSFL, aligning with both parallel and perpendicular directions to the polarization. In the central region of the irradiated area, barely visible $HSFL_{\perp}$ structures are observed (as shown in the top right insets of Fig. 1) with an orientation perpendicular to the **E**, owing to the high local fluence interacting with the substrate. It is essential to highlight the existence of a transitional (melted) region between the central and peripheral areas of the laser spot, where parallel $HSFL_{II}$ are observed relative to E (presented in the bottom left insets of Fig. 1). In this melted region, atoms from the thin film locally contribute to the formation of $HSFL_{II}$ due to its partial presence, even when the laser beam interacts with the glass substrate. An interesting observation is the presence of an intermediate region resembling nanosquares situated between parallel and perpendicular HSFL structures (presented in the middle right insets of Fig. 1). This can be attributed to the overlap between the two types of HSFL on the glass substrate, as depicted in the middle right side of Fig. 1. The transition from parallel to perpendicular LIPSS structures was observed by Höhm *et al.*[24] on a dielectric SiO_2 substrate, achieved by increasing the laser fluence. Karim *et al.*[25] observed similar overlapping structures between the two $LSFL_{II}$ and $LSFL_{\perp}$ patterns on the surface of gadolinium-doped ceria (GDC) thin films using a picosecond (Nd:YAG) laser operating at its third harmonic (λ = 355 nm). These intermediate or overlapping structures may have originated from a higher energy distribution over the same ablated area. As most dielectric materials display

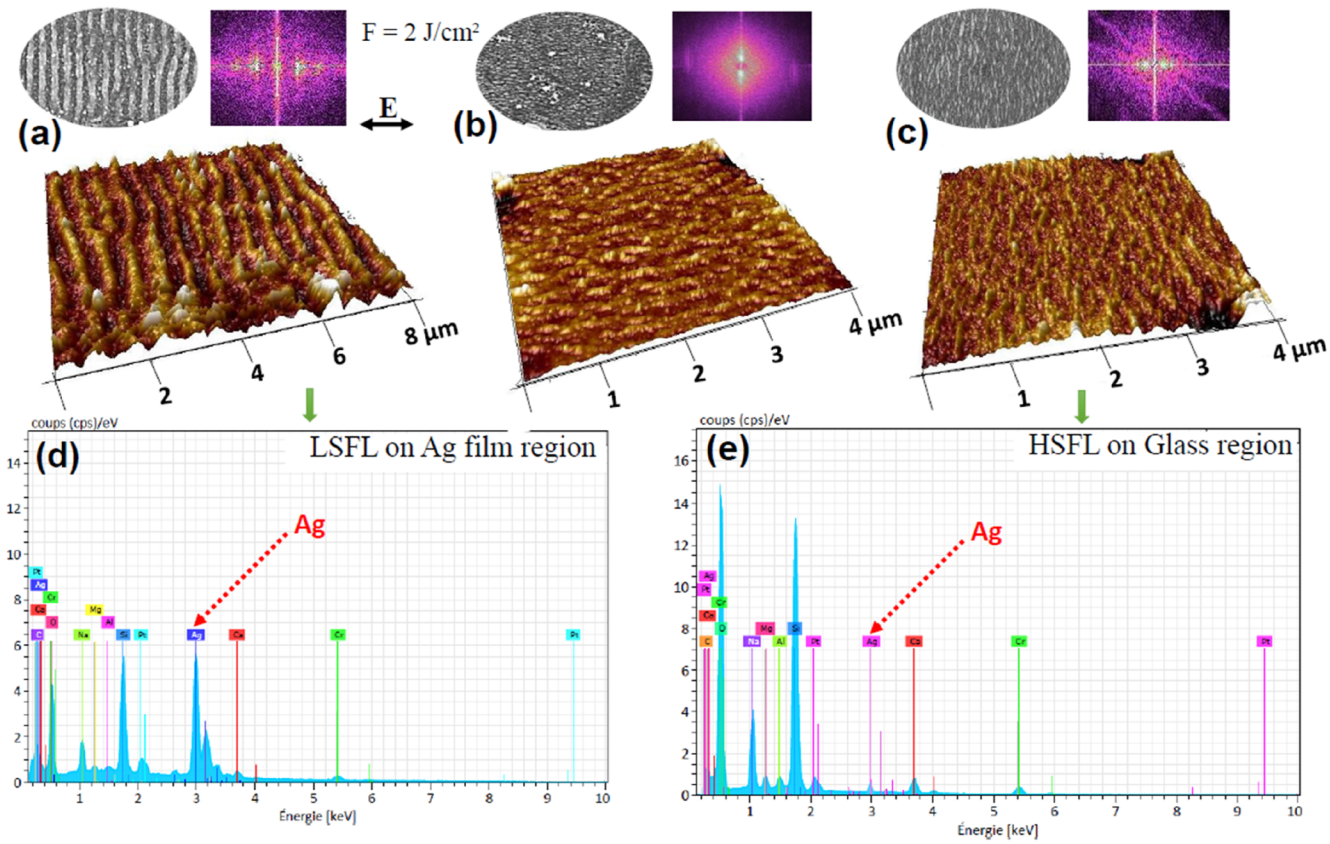

FIG. 2. AFM images of the LIPSS formation at E = 10 μJ at 515 nm with corresponding SEM and 2D-FFT results. The observed AFM images along with the 2D-FFT are presented: (a) $LSFL_{\perp}$ on thin film; (b) $HSFL_{II}$ on glass in the melted region; and (c) $HSFL_{\perp}$ on glass in the center of the ablated area. The EDX compositions are provided for (d) $LSFL_{\perp}$ on the thin film and (e) $HSFL_{\perp}$ on the glass region.

pronounced incubation behavior, the appearance of different types of LIPSS is attributed to electromagnetic scattering mechanisms such as near-field and far-field surface scattering, along with laser beam interference.[26] In addition, the number of pulses and the incident laser fluence can significantly influence this phenomenon. This overlapping phenomenon contributes to the formation of nanosquare features at higher energy densities or fluences.

Figures 2(a)–2(c) depict magnified LIPSS structures captured in both SEM and AFM images, corresponding to thin film and glass surfaces, respectively. The estimated spatial period (Λ) of the $LSFL_{\perp}$ exposed on the Ag thin film is ~400 nm, oriented perpendicular to the direction of **E**, as depicted in Fig. 2(a). This aligns well with the literature, indicating that the LSFL period size (Λ_{LSFL}) closely approximates or is slightly smaller than the irradiation wavelength (λ) when applied to dielectric material surfaces, oriented perpendicular to the polarization.[27,28] Figures 2(b) and 2(c) depict the formation of HSFL on the glass substrate in both parallel and perpendicular directions to the **E**, respectively. The estimated Λ_{HSFL} for these two distinct types of perpendicular and parallel structures ranges between 110 and 85 nm, respectively. 2D-fast Fourier transform (2D-FFT) images of a large area reveal the periodicity of both LSFL and HSFL structures, as shown in Figs. 2(a)–2(c). The periodicity of LIPSS observed in the FFT image is consistent with the results from SEM/AFM analyses. It is widely acknowledged that the spatial periods of HSFL, which are predominantly observed in dielectric materials, are significantly smaller than the beam wavelength ($\Lambda_{HSFL-II} < \lambda/2$). These structures are often oriented perpendicular to the polarization,[29] sometimes parallel to it.[30]

We used energy dispersive x-ray spectroscopy (EDX) to confirm the elemental compositions in both LSFL and HSFL regions. According to the EDX measurement, the $LSFL_{\perp}$ region predominantly exhibits signals from silver (Ag) along with O and Si, confirming the presence of the metal thin film as shown in Fig. 2(d). Conversely, the $HSFL_{\perp}$ predominantly shows signals from O and Si [Fig. 2(e)], along with other glass components such as Na, Mg, Al, and Ca, indicating their origin from the soda-lime glass substrate. In addition, weak signals from Ag and Cr are observed in Fig. 2(e), representing their removal during laser irradiation. Both EDX spectra display a platinum (Pt) peak, evidencing the sputtered Pt thin-film layer used for the SEM measurement.

B. Glass texturing and HSFL formation at higher pulse energy

Figures 3(a)–3(d) illustrate the SEM observations of a thin-film-deposited glass substrate with different repetition rates (f) ranging from 10 to 250 kHz at 15 μJ. The resulting image has an elliptical shape or an annular structure under all irradiated conditions when the spot size is about 60 μm. The circular shape observed at 10 μJ (Fig. 1) undergoes a complete transformation into an elliptical shape when the energy is increased to 15 μJ (Fig. 3), causing a corresponding increase in the spot size from 35 to 60 μm. In this instance, the energy distribution does not significantly affect the ablated area; instead, there is an uneven distribution of energy over the surface. Hence, we were unable to observe any regular periodic structures on the Ag film surface. Moreover, the formation of irregular structures in the central area (glass substrate) is evidenced due to insufficient fluence at 10 kHz. These structures may form upon irradiation due to a melting and successive resolidification process, and occur predominantly in the region impacted by the most intense part of the laser beam.[31] Hu *et al.*[31] observed similar structures on a Bi_2Te_3 single crystal under fs-laser irradiation at 800 nm when the energy was increased to 20 μJ, while Danilov *et al.*[18] observed the same elliptically melted Ag thin film under fs-laser irradiation at 515 nm when

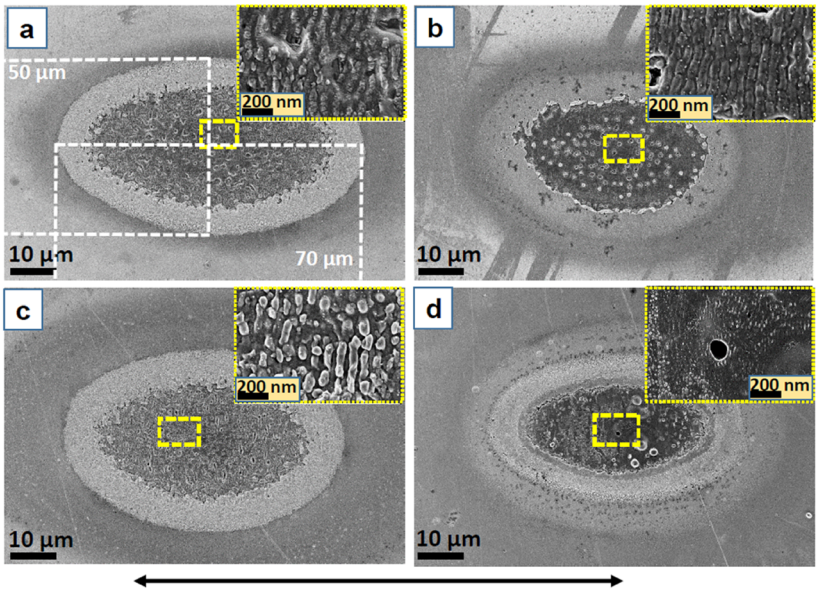

FIG. 3. (a)–(d) SEM images of the surface of thin-film-influenced soda-lime glass upon irradiation with different repetition rates of 10, 50, 100, and 250 kHz, respectively, at 15 μJ. The black arrow indicates the direction of the electric field vector.

the energy was increased to 1.32 μJ. The repetition of multiple pulses at 10 kHz induces the creation of structural patterns, characterized by the formation of irregular LIPSS concentrated in the center, as depicted in Fig. 3(a). Within the ablation area, two distinct regions were observed: (i) an inner region marked by the selective removal of the thin film, and (ii) an outer region where the absence of thin film removal was apparent. Notably, circular micropit structures, resembling bubbles, begin to form over the HSFL regime, with diameters in the micrometer range. Farid *et al.*[21] reported the ablation of ITO thin film (175 nm) by a femtosecond-IR laser beam and observed the selective removal of the ITO film layer on glass without any damage to the underlying glass surface. This selective removal is attributed to the low energy doses or insufficient thermal energy in the targeted region. An increase in the repetition rate to 50 kHz results in the formation of regular HSFL on the glass substrate, accompanied by the appearance of elliptical thin walls, where regions of film peeling from the glass substrate are noticeable in Fig. 3(b). Moreover, the size and density of the micropits increased due to the increase in the redeposition of nanoparticles. When the frequency reaches 100 kHz, the micropits in the central region of the irradiated area begin to overlap, and the LIPSS pattern becomes distorted, as illustrated in Fig. 3(c). Previous studies suggest that this morphological feature may be attributed to thermal effects occurring during the ablation process. Lian *et al.*[32] observed similar elliptical structures with micropits (bubbles) in the central area of ablation on a Ti thin layer under fs-laser irradiation. They suggested that the removal of the liquid phase at the bottom leads to the formation of micro-sized bubbles. However, at a higher f of 250 kHz, the occurrence of LIPSS has almost disappeared, while a large hole has formed in the center on the glass substrate, as depicted in Fig. 3(d). This phenomenon may originate when the laser pulse energy or repletion rate is close to its maximum, and it appears to be associated with the propagation of the shock wave.[18] In all instances, HSFL observed on the glass substrate exhibit an orientation perpendicular to the **E**, consistent with expectations for dielectric materials.

C. Discussion of LIPSS formation

In metals or semiconducting materials, LSFL can be attributed to the excitation of surface plasmon polaritons (SPPs) on the surface or within thin film layers. In the case of dielectric materials, HSFL are predominantly formed with reduced periodicity. According to the Sipe theory, the LIPSS formation on dielectric materials is attributed to the interaction of the laser radiation with surface defects and inhomogeneities, leading to the generation of radiation remnants (RR).[8] In our case, a dielectric glass substrate coated with a metal thin film involves interference between the incident light and the electromagnetic wave of the thin-film layer mediated by SPPs, as depicted in Fig. 4. In this mechanism, when a laser beam interacts with a metal film, the energy from the light is absorbed by the free electrons in the conduction band (CB). Through multi-photon absorption, this energy can be sufficient to excite the electrons to higher energy states or even into the valence band (VB), depending on the photon energy of the material. This electron transition can potentially generate electromagnetic waves on the substrate surface due to surface plasmon polaritons (SPPs), which leads to the LIPSS formation. This LIPSS formation process similarly determines the mechanisms on metals or semiconductors, induced by SPPs on a glass substrate through thin-film absorption. The metal thin-film layer was gradually removed with higher pulse numbers as the repetition rate increased, leading to a reduction in periodicity size to below half the incident wavelength, namely, as HSFL. The formation of HSFL is widely accepted to be attributed to the potential factor of self-organization.[30]

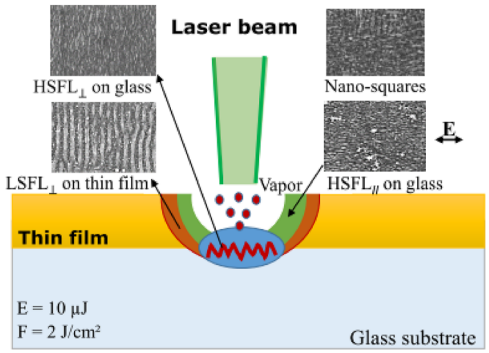

FIG. 4. Schematic representation of the possible mechanisms for LIPSS formation at 515 nm.

D. Comparative analysis of LIPSS and surface texturing

A complete analysis of the LIPSS formation and glass texturing was conducted for various repetition rates and pulse energies, using a wavelength of 515 nm and a pulse duration of 300 fs. Figure 5 presents SEM images of the thin-film-coated glass substrate obtained under various laser energies (10, 15, and 20 μJ) and repetition rates (10, 100, and 250 kHz). At 10 μJ, the absence of the LIPSS formation on the metal film surface is attributed to an insufficient energy distribution at a repetition rate of 10 kHz. As the repetition rate increases to 100 kHz, perpendicular HSFL$_\perp$ were observed on the glass substrate, as discussed in Sec. III A. A subsequent increase in f = 250 kHz induced a transformation in HSFL orientation from perpendicular to parallel to the laser beam polarization, **E**. This could be attributed to the change in energy distribution across the ablated area caused by the coupling between the metal film and the glass substrate. At 15 μJ, the formation of irregular HSFL$_\perp$ was observed at 10 kHz. As f increases to 100 kHz, the HSFL$_\perp$ began to show signs of disorder, and at 250 kHz, the LIPSS nearly disappeared due to glass texturing, as detailed in Sec. III B. At the maximum pulse energy of 20 μJ, highly regular HSFL$_\perp$ were formed on the glass substrate at 10 kHz. When f was increased to 100 kHz, the HSFL orientation transformed from perpendicular to parallel, similar to the behavior observed at 10 μJ. However, at a higher f of 250 kHz, the LIPSS formation almost disappeared, and a large hole was formed at the center of the glass substrate, confirming glass texturing.

We also presented a mapping of the laser-induced surface modification of the thin-film-coated glass substrate as suggested in Fig. 6, as laser energy and repetition rates are varied from 10 to 20 μJ and from 10 to 500 kHz, respectively. In Fig. 6, the square, star, triangle, and rhombus symbols correspond to the absence of LIPSS, perpendicular HSFL$_\perp$, parallel HSFL$_{II}$, and glass texturing,

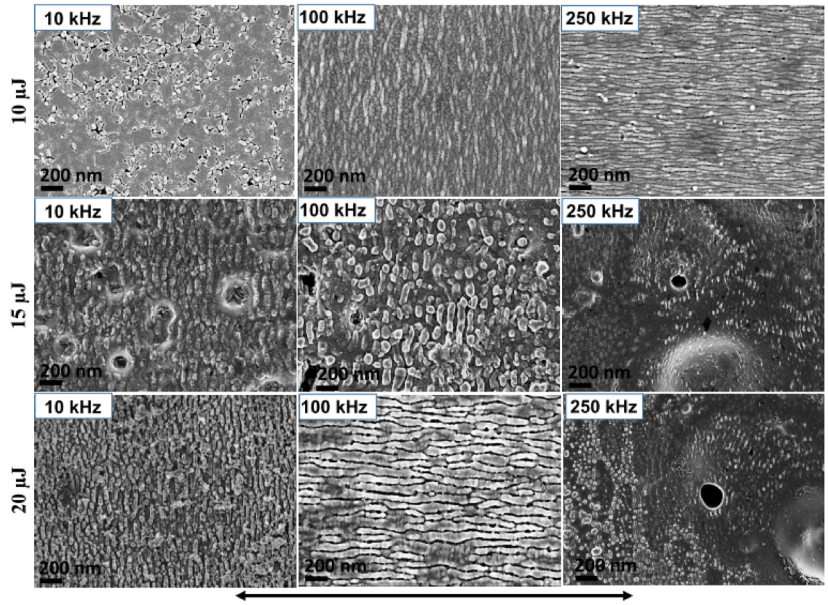

FIG. 5. SEM images of the thin-film-coated soda-lime glass surface after irradiation with different repetition rates (10, 100, and 250 kHz) are shown. The images are arranged in rows corresponding to three different energies: 10 (top), 15 (middle), and 20 μJ (bottom). The black arrow indicates the direction of the electric field vector or polarization.

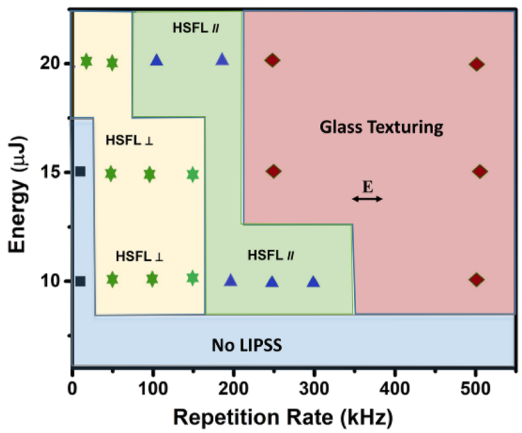

FIG. 6. A mapping of the Green (515 nm)-wavelength-induced surface modification of thin-film-coated soda-lime glass for different energies (μJ) and repetition rates (kHz).

respectively. From the comparative analysis, we found that the LIPSS formation is possible up to 100 kHz for the energy range from 10 to 20 μJ. At higher repetition rates, surface texturing intensifies owing to the large number of pulses.

IV. CONCLUSIONS

A one-step (static mode) femtosecond laser processing method using a 515 nm laser beam has successfully generated sub-100 nm LIPSS on a soda-lime glass substrate. The new insight from the present observation is the formation of LSFL on the thin film and two distinct types of HSFL on the glass substrate at a pulse energy of 10 μJ. The transient changes in surface morphology within each pulse play a crucial role in the formation of LSFL on the thin film, with a period size of ~400 nm, and HSFL on the glass substrate, with a period size of ~110 nm. Elemental analysis (EDX) confirmed strong signals from Si and O, indicating the presence of the glass substrate (HSFL region), while detecting minimal signals from the thin film of Ag and Cr. In contrast, the LSFL region exhibits a strong signal from Ag, compared to the glass compounds, confirming the presence of the metal film surface. Another interesting result is that the laser spot shape changed from circular to elliptical as the laser energy increased from 10 to 15 μJ, leading to the formation of irregular surface structures. This transition could be attributed to the uneven energy distribution across the ablated area of the material surface. A novel aspect of this study is the successful comparative analysis of surface modifications on metal thin-film-coated glass substrates, conducted across varying repetition rates and energy levels. A mapping image has been provided to enhance the understanding of the LIPSS formation and glass texturing. Using sequences of ultra-short laser pulses with varying repetition rates provides a novel approach to manipulating LIPSS patterns, particularly on cost-effective soda-lime glass. This study found that the LIPSS formation is feasible up to 100 kHz within the energy range of 10–20 μJ. However, further investigation is needed to explore the effects of increasing the energy level beyond 20 μJ in the future.

ACKNOWLEDGMENTS

The authors acknowledge the financial support from the Région Center Val de Loire within the framework of the ARD MATEX-SAILOR project.

AUTHOR DECLARATIONS

Conflict of Interest

The authors have no conflicts to disclose.

Author Contributions

K. Deva Arun Kumar: Conceptualization (equal); Data curation (equal); Investigation (equal); Methodology (equal); Visualization (equal); Writing – original draft (equal). **Barthélemy Aspe**: Data curation (equal); Investigation (equal); Validation (equal); Writing – review & editing (equal). **Martin Depardieu**: Data curation (equal); Investigation (equal); Methodology (equal); Project administration (equal); Writing – review & editing (equal). **Anne-Lise Thomann**: Data curation (equal); Investigation (equal); Methodology (equal); Writing – review & editing (equal). **Nadjib Semmar**: Conceptualization (lead); Data curation (equal); Funding acquisition (lead); Investigation (equal); Methodology (equal); Project administration (lead); Validation (equal); Visualization (equal); Writing – review & editing (equal).

DATA AVAILABILITY

The data that support the findings of this study are available from the corresponding author upon reasonable request.

REFERENCES

[1] C. McDonnell, D. Milne, H. Chan, D. Rostohar, and G. M. O'Connor, "Part 2: Ultra-short pulse laser patterning of very thin indium tin oxide on glass substrates," Opt. Lasers Eng. **81**, 70–78 (2016).

[2] F. Ruffino and M. G. Grimaldi, "Nanostructuration of thin metal films by pulsed laser irradiations: A review," Nanomaterials **9**(8), 1133 (2019).

[3] K. Ahmmed, C. Grambow, and A.-M. Kietzig, "Fabrication of micro/nano structures on metals by femtosecond laser micromachining," Micromachines **5**(4), 1219–1253 (2014).

[4] A. Y. Vorobyev and C. Guo, "Direct femtosecond laser surface nano/microstructuring and its applications," Laser Photonics Rev. **7**(3), 385–407 (2013).

[5] Y. Shimotsuma, P. G. Kazansky, J. R. Qiu, and K. Hirao, "Self-organized nanogratings in glass irradiated by ultrashort light pulses," Phys. Rev. Lett. **91**, 247405 (2003).

[6] K. C. Phillips, H. H. Gandhi, E. Mazur, and S. K. Sundaram, "Ultrafast laser processing of materials: A review," Adv. Opt. Photonics **7**, 684–712 (2015).

[7] P. Bizi-Bandoki, S. Benayoun, S. Valette *et al.*, "Modifications of roughness and wettability properties of metals induced by femtosecond laser treatment," Appl. Surf. Sci. **257**, 5213–5218 (2011).

[8] K. D. A. Kumar, A. Capelle, W. Karim, H. Rabat, L. Gimenez, B. Aspe, A. Caillard, M. Depardieu, A.-L. Thomann, and N. Semmar, "Thin film mediated and direct observation of LIPSS on soda-lime glass by femtosecond IR laser beam," Opt. Lasers Eng. **180**, 108321 (2024).

[9] P. Temple and M. Soileau, "Polarization charge model for laser-induced ripple patterns in dielectric materials," IEEE J. Quantum Electron. **17**, 2067 (1981).

[10] D. Dufft, A. Rosenfeld, S. K. Das, R. Grunwald, and J. Bonse, "Femtosecond laser-induced periodic surface structures revisited: A comparative study on zno," J. Appl. Phys. **105**, 034908 (2009).

[11] A. Borowiec and H. K. Haugen, "Subwavelength ripple formation on the surfaces of compound semiconductors irradiated with femtosecond laser pulses," Appl. Phys. Lett. **82**, 4462–4464 (2003).

[12] A. Rosenfeld, M. Rohloff, S. Hohm, J. Krüger, and J. Bonse, "Formation of laser-induced periodic surface structures on fused silica upon multiple parallel polarized double- femtosecond-laser-pulse irradiation sequences," Appl. Surf. Sci. **258**(23), 9233–9236 (2012).

[13] Q. Sun, F. Liang, R. Vallée, and S. L. Chin, "Nanograting formation on the surface of silica glass by scanning focused femtosecond laser pulses," Opt. Lett. **33**(22), 2713–2715 (2008).

[14] S. Graf, C. Kunz, and F. Müller, "Formation and properties of laser-induced periodic surface structures on different glasses," Materials **10**, 933 (2017).

[15] T. Maeder, "Review of Bi_2O_3 based glasses for electronics and related applications," Int. Mater. Rev. **58**, 3–40 (2013).

[16] E. Kilinc and R. J. Hand, "Mechanical properties of soda-lime-silica glasses with varying alkaline earth contents," J. Non-Cryst. Solids **429**, 190–197 (2015).

[17] E. V. Kuzmin and A. V. Klekovkin, "Features of structuring and ablation of thin titanium films by femtosecond laser pulses," Opt. Spectrosc. **131**(9), 857–861 (2023).

[18] P. A. Danilov, A. A. Ionin, S. I. Kudryashov, A. A. Rudenko, N. A. Smirnov, A. P. Porfirev, A. A. Kuchmizhak, O. B. Vitrik, M. S. Kovalev, and G. K. Krasin, "Femtosecond laser ablation of thin silver films in air and water under tight focusing," Opt. Mater. Express **10**, 2717–2722 (2020).

[19] A. Danilov, D. A. Zayarnyi, A. A. Ionin, S. I. Kudryashov, S. V. Makarov, A. A. Rudenko, V. I. Yurovskikh, Y. N. Kulchin, O. B. Vitrik, A. A. Kuchmizhak, E. A. Drozdova, and S. B. Odinokov, "Mechanisms of formation of sub- and micrometre-scale holes in thin metal films by single nano- and femtosecond laser pulses," Quantum Electron. **44**(6), 540–546 (2014).

[20] J. Sládek, K. Hlinomaz, I. Mirza, Y. Levy, T. Derrien, M. Cimrman, S. S. Nagisetty, J. Čermák, T. H. Stuchlíková, J. Stuchlík, and N. M. Bulgakova, "Highly regular LIPSS on thin molybdenum films: Optimization and generic criteria," Materials **16**(7), 2883 (2023).

[21] N. Farid, H. Chan, D. Milne, A. Brunton, and G. M. O'Connor, "Stress assisted selective ablation of ITO thin film by picosecond laser," Appl. Surf. Sci. **427**, 499–504 (2018).

[22] A. V. Dostovalov, T. Derrien, S. A. Lizunov, F. Přeučil, K. A. Okotrub, T. Mocek, V. P. Korolkov, S. A. Babin, and N. M. Bulgakova, "LIPSS on thin metallic films: New insights from multiplicity of laser-excited electromagnetic modes and efficiency of metal oxidation," Appl. Surf. Sci. **491**, 650–658 (2019).

[23] B. Öktem *et al.*, "Nonlinear laser lithography for indefinitely large-area nanostructuring with femtosecond pulses," Nat. Photonics **7**(11), 897–901 (2013).

[24] S. Höhm, A. Rosenfeld, J. Krüger, and J. Bonse, "Femtosecond laser-induced periodic surface structures on silica," J. Appl. Phys. **112**, 014901 (2012).

[25] W. Karim, A. Petit, H. Rabat, M. Tabbal, A.-L. Thomann, and N. Semmar, "Picosecond laser beam nanostructuring of GDC thin films: Exchange surface enhancement by LIPSS," Appl. Phys. A **128**, 731 (2022).

[26] J. Bonse and S. Gräf, "Maxwell meets Marangoni—A review of theories on laser-induced periodic surface structures," Laser Photonics Rev. **14**(10), 2000215 (2020).

[27] A. Y. Vorobyev, V. S. Makin, and C. Guo, "Periodic ordering of random surface nanostructures induced by femtosecond laser pulses on metals," J. Appl. Phys. **101**, 034903 (2007).

[28] J. Bonse, H. Sturm, D. Schmidt, and W. Kautek, "Chemical, morphological and accumulation phenomena in ultrashort-pulse laser ablation of TiN in air," Appl. Phys. A: Mater. Sci. Process. **71**, 657–665 (2000).

[29] M. Rohloff, S. K. Das, S. Höhm, R. Grunwald, A. Rosenfeld, J. Krüger, and J. Bonse, "Formation of laser-induced periodic surface structures on fused silica upon multiple cross-polarized double-femtosecond-laser-pulse irradiation sequences," J. Appl. Phys. **110**, 014910 (2011).

[30] J. Bonse, J. Krüger, S. Höhm, and A. Rosenfeld, "Femtosecond laser-induced periodic surface structures," J. Laser Appl. **24**, 042006 (2012).

[31] M. Hu, J. JJ Nivas, M. Salvatore, S. L. Oscurato, A. Guarino, R. Fittipaldi, S. Amoruso, and A. Vecchione, "Femtosecond laser-induced periodic surface structuring of the topological insulator bismuth telluride," Adv. Phys. Res. **2**, 2300049 (2023).

[32] Y. Lian, L. Jiang, J. Sun, W. Tao, Z. Chen, G. Lin, Z. Ning, and M. Ye, "Ultrafast dynamics and ablation mechanism in femtosecond laser irradiated Au/Ti bilayer systems," Nanophotonics **12**(24), 4461–4473 (2023).